CHAPTER V
EFFECT OF TITANIUM PRECUSSOR ON DEHYDRIDING/HYDRIDING OF SODIUM ALANATE

5.1 Abstract

$TiCl_3$ has been considered as the best catalyst for hydrogen desorption/re-absorption of $NaAlH_4$ in terms of kinetic enhancement. However, the formation of NaCl as a by-product leads to the incomplete hydrogen re-absorption of $NaAlH_4$. In this work, TiO_2 and metallic Ti were selected as catalysts for the reaction to avoid the formation of the by-product. It was found that TiO_2 doped $NaAlH_4$ exhibits the similar behavior as $TiCl_3$ doped $NaAlH_4$ with the reversible hydrogen capacity about 3.8 wt% (H/M). In addition, TiO_2 also improves the rate of hydrogen re-absorption in the desorbed sample. This is due to the porosity of TiO_2 facilitates the hydrogen diffusion in the desorbed sample. However, some TiO_2 is reduced by $NaAlH_4$ and produces sodium oxide and hydroxide as by-products. This may be a reason why the reversible hydrogen capacity of $NaAlH_4$ doped with TiO_2 is not different from that of $TiCl_3$ doped $NaAlH_4$. Unexpectedly, metallic Ti doped $NaAlH_4$ shows the inferior hydrogen desorption/re-absorption. Its hydrogen reversible capacity is around 1 wt% (H/M). The formation of TiH_x ($1 < x < 2$) was detected in the sample after hydrogen desorption/re-absorption. This may be attributed to the formation of TiH_x that decreases the activity of hydrogen dissociation in the desorbed sample.

5.2 Introduction

The storage of hydrogen in complex metal hydride has been the subject for extensive research for many years. However, no hydride system fulfills strict requirements with respect to safety, reversible hydrogen capacity, and kinetics for commercial vehicular applications [1-2]. Sodium alanate or sodium aluminium hydride ($NaAlH_4$) has shown promising properties for hydrogen storage after the discovery on its reversibility with the presence of a metal catalyst [3-11]. Thus, this complex metal hydride system has been considered as a model system for hydrogen

storage material development. Ti-based catalysts have been widely studied and reported to be the best in improving the hydrogen desorption/re-absorption of $NaAlH_4$, but so far the reversible hydrogen capacity cannot reach its original state. The maximum reversible hydrogen capacity is close to 4 wt% H_2 compared to 5.6 wt% H_2 achieved from the first desorption of $NaAlH_4$ [8]. $Ti(BuO)_4$ was first introduced as a catalyst in the hydrogen desorption/re-absorption of $NaAlH_4$ [3]. Contaminant gases like propane and butane were produced along with hydrogen from the decomposition of the alkoxide compound. Moreover, oxygen from the alkoxide catalyst also contaminated the surface of the hydride and lowered reversible hydrogen capacity [12]. To avoid the problem, Ti-based halide compounds such as $TiCl_3$ was used as a catalyst. Although $TiCl_3$ shows better performance than $Ti(BuO)_4$, the reversible hydrogen capacity is still not up to 5.6 wt% H_2. In our previous work, we studied the hydrogen desorption/re-absorption of $NaAlH_4$ doped with different transition metal chlorides [10-11]. $TiCl_3$ was found to be the best catalyst among the tested four transition metal chlorides with the reversible hydrogen capacity about 3.5 wt% H_2 (3.85 wt% H_2 based on hydride weight). Doping $TiCl_3$ in the hydride system poses the formation of NaCl as a by-product, which consumes active Na in the hydride system and may be one of the reasons for the low reversible hydrogen capacity of $NaAlH_4$.

To further substantiate whether the formation of the by-product during the hydrogen desorption/re-absorption causes the decrease in the reversible hydrogen capacity, TiO_2 and metallic Ti were used as catalysts in the hydrogen desorption/re-absorption of $NaAlH_4$ compared with that using $TiCl_3$. Moreover, the isothermal hydrogen desorption of $TiCl_3$ doped $NaAlH_4$ was conducted and fitted to the Arrhenius equation to determine the pre-exponential rate constant and activation energy.

5.3 Experimental

5.3.1 Materials

$NaAlH_4$ (90% purity), Ti powder (99.98%, 325 mesh) were purchased from Aldrich Chemical. TiO_2 (P25) was ordered from Degüssa. $TiCl_3$ (Riedel-de

Haën) was obtained from vacuum drying of 12% $TiCl_3$ in hydrochloric acid (see detail of preparation in Chapter 3).

5.3.2 Hydrogen desorption/absorption

$NaAlH_4$, metallic Ti, and TiO_2 were used as received. The hydride sample was prepared by adding $NaAlH_4$ with 4 mol% metallic Ti, TiO_2, or $TiCl_3$ using a centrifugal ball mill (Retsch ball mill model S100, stainless steel vial size 250 ml, 1: 200 the mass ratio of sample and milling ball) for 20 min with a speed of 300 rpm. All sample preparation and the milling process were conducted under nitrogen atmosphere.

Hydrogen desorption/absorption on samples was measured by thermovolumetric method (Sievert's apparatus) as shown in Figure 4.1. Immediately after mixing, approximately 1 g of a sample was transferred into the high pressure stainless steel reactor in the glove box. Then, the reactor was fixed with the Sievert's apparatus. The K-type thermocouple was placed inside the reactor to measure the temperature connected with a PID temperature controller and furnace. The pressure transducer (Cole Parmer, model 68073-68074) was used to measure the pressure change resulting from hydrogen desorption from the sample. For hydrogen desorption, the samples were heated from room temperature to 280°C with a heating rate of 3°C min^{-1}. For the absorption experiments, hydrogen (99.9995%) was used to pressurize the high pressure vessel at 120°C and 10 MPa for 10 h. Once the pressure reading was constant over a period of time, the data was used to calculate the amount of hydrogen absorbed on the sample. An amount of the released hydrogen shown in the results (H/M) was calculated with respect to the amount of $NaAlH_4$ in the sample. The same procedure was repeated to investigate their reversibility.

To determine the pre-exponential factor of frequency factor, A, and activation energy, Ea, from the Arrhenius equation (Eq. (5.1)), the hydrogen desorptions were performed at a constant temperature 80, 90, 105, 115, and 135°C for $TiCl_3$ doped $NaAlH_4$; and 180, 190, 200, and 210°C for $TiCl_3$ doped Na_3AlH_6.

Sample characterization was also performed using a Rigaku x-ray diffractometer at room temperature over a range of diffraction angles from 28-80 with CuK-alpha radiation (40 kV, 30 mA). The oxidation state of TiO_2 was detected

by electron spin resonance (ESR) spectrometer (JEO model JES-RE2X, frequency 88-96 GHz). And the surface area of the samples were determined by nitrogen adsorption/desorption at 77K (Micrometrics Tristar Surface analyzer) with Brunauer-Emmet-Teller (BET) analysis.

$$k = A\exp\left(\frac{-Ea}{RT}\right) \tag{5.1}$$

5.4 Results and Discussion

5.4.1 Hydrogen desorption/absorption on doped $NaAlH_4$

Figure 5.1 shows the temperature program desorption in the 1st cycle of $NaAlH_4$ doped with 4 mol% metallic Ti (Ti-$NaAlH_4$), $NaAlH_4$ doped with 4 mol% TiO_2 (TiO_2-$NaAlH_4$), and $NaAlH_4$ doped with 4 mol% $TiCl_3$ ($TiCl_3$-$NaAlH_4$). Surprisingly, it can be clearly observed that the hydrogen desorption behavior of $TiCl_3$-$NaAlH_4$ is quite similar with that of TiO_2-$NaAlH_4$ by starting to decompose at 110°C while the hydrogen desorption of Ti-$NaAlH_4$ occurs at significantly higher temperature, 160°C. Figure 5.2 displays the reversibility of TiO_2-$NaAlH_4$. The subsequent hydrogen desorption behavior reproduces that of the 1st desorption except the reversible hydrogen capacity is lower, 3.8 wt% (H/M). In contrast, the subsequent hydrogen desorption of Ti-$NaAlH_4$ shifts to higher temperature, 200°C, while the reversible hydrogen re-absorption is around 1 wt% (H/M), Figure 5.3. From the sharp increase of subsequent desorption profiles, it indicates that only the 2nd step of the reaction re-absorbs hydrogen (Eq. (5.2)). Thus, this answers why the subsequent hydrogen desorption takes place at higher temperature than that of the first desorption cycle. In addition, almost no significant changes in the amount of the desorbed hydrogen in the subsequent cycles even after 7 cycles for TiO_2-$NaAlH_4$ and Ti-$NaAlH_4$. This result is in good agreement with the sample doped with $TiCl_3$ as shown in Figure 4.4.

$$3NaH + Al + \frac{3}{2}H_2 \leftrightarrow Na_3AlH_6 \tag{5.2}$$

Figure 5.4 is the comparison of the hydrogen desorption in the 7th desorption of a) TiO_2-$NaAlH_4$, b) $TiCl_3$-$NaAlH_4$, and c) Ti-$NaAlH_4$. Again, it clearly shows that the behavior of hydrogen desorption of TiO_2-$NaAlH_4$ is almost identical to that of $TiCl_3$-$NaAlH_4$. This reveals that TiO_2 exhibits the same effect as $TiCl_3$ in catalyzing the hydrogen desorption/re-absorption of $NaAlH_4$.

The comparison of the hydrogen re-absorption as shown in Figure 5.5 shows that TiO_2-$NaAlH_4$ has the highest hydrogen re-absorption rate among the tested samples. The magnitude of the initial rate of hydrogen re-absorption of TiO_2-$NaAlH_4$ (0.18 wt% (H/M) min^{-1}) is higher than that of $TiCl_3$-$NaAlH_4$ (0.07 wt% (H/M) min^{-1}). TiO_2-$NaAlH_4$ takes 5 h to reach the highest hydrogen re-absorption while $TiCl_3$-$NaAlH_4$ needs 6 h to do so. In the case of Ti-$NaAlH_4$, its hydrogen re-absorption cannot reach as high even after 10 h. This result is in good agreement with the low hydrogen capacity in the subsequent cycles of Ti-$NaAlH_4$. The inferior hydrogen re-absorption rate of $TiCl_3$-$NaAlH_4$ compared with TiO_2-$NaAlH_4$ may be because the porous structure of TiO_2 increases the void in the hydride sample and prevent the agglomeration of the desorbed sample. This assists in increasing the surface area of the bulk hydride system.

To support this hypothesis, the BET surface area analysis was conducted with the desorbed samples of TiO_2-$NaAlH_4$ and $TiCl_3$-$NaAlH_4$. The surface area of the desorbed sample doped with TiO_2 is 147.65 m^2 g^{-1} while that of the desorbed sample doped with $TiCl_3$ is 56.76 m^2 g^{-1}. Thus, it can be deduced that not only does TiO_2 improve the hydrogen reversibility of $NaAlH_4$, its porosity and high surface area also increase the surface area of the hydride sample, which facilitates the hydrogen diffusion in the desorbed sample. This leads to better hydrogen re-absorption of the TiO_2-$NaAlH_4$ sample than that of the $TiCl_3$-$NaAlH_4$ sample.

5.4.2 X-ray diffractions of doped $NaAlH_4$

In addition to the question on how TiO_2 catalyzes the reversible reaction of $NaAlH_4$, the TiO_2-$NaAlH_4$ sample was characterized by the XRD technique as shown in Figure 5.6. After milling, the XRD result reveals only the

pattern of $NaAlH_4$ while after complete hydrogen desorption, the products contain Al and NaH together with NaOH and Na_2O. The reabsorbed sample consists of $NaAlH_4$, Al, and a small amount of Na_3AlH_6 together with Na_2O. The formation of oxide compound in the system indicates that some TiO_2 is reduced by $NaAlH_4$ to produce oxygen and form NaOH and Na_2O in the hydride system. No evidence of Ti-compound was detected by XRD. To confirm the reduction of TiO_2 by $NaAlH_4$, the TiO_2-$NaAlH_4$ sample was analyzed by ESR spectrometer. From the ESR spectrum shown in Figure 5.7, the signal of Ti^{3+} reveals that some TiO_2 was reduced from Ti^{4+} as Ti^{3+}. This evidence implies that there are the defect sites on the surface of TiO_2, which acts as the active sites for hydrogen dissociation into the desorbed sample [13]. However, the produced oxide compound also decreases the reversible hydrogen capacity of the hydride system.

Figure 5.8 shows the XRD patterns of the Ti-$NaAlH_4$ sample. After milling, peaks of $NaAlH_4$ with small peaks of metallic Ti can be observed. Then, metallic Ti becomes TiH_x ($1 < x < 2$) after hydrogen desorption/re-absorption. Moreover, no evidence of $NaAlH_4$ peaks in the sample after hydrogen re-absorption, only peaks of Na_3AlH_6, Al, and TiH_x can be observed. This result is in good agreement with the subsequent hydrogen desorption behavior of Ti-$NaAlH_4$ (Figure 5.3(b)). The formation of TiH_x corresponds to the drop in the activity of Ti in catalyzing the hydrogen dissociation leading to the lower hydrogen re-absorption.

5.4.3 Arrhenius analysis of $TiCl_3$-$NaAlH_4$

Correlation between time and amount of released hydrogen at constant temperature is shown in Figure 5.9 for the decomposition of $NaAlH_4$ to Na_3AlH_6 and Al; and in Figure 5.10 for the decomposition of Na_3AlH_6 to NaH and Al. From the result, the higher desorption temperature, the higher the hydrogen desorption rate. That observation is the same for both 1st and 2nd step desorption. The maximum reversible capacity in the 1st step of reaction is around 2.6 wt% (H/M). The hydrogen desorption take places at temperature of 135°C to reach the highest capacity in the 1st step within 20 min. In the case of the 2nd decomposition, the release of hydrogen takes lower than 20 min at the desorption temperature higher than 190°C to reach the maximum hydrogen capacity of 1.2 wt% (H/M).

Figure 5.11 shows the Arrhenius plot of $NaAlH_4$ [7] and 4 mol% $TiCl_3$ doped $NaAlH_4$. From the slope and interception of the plot, calculated Ea and A are displayed in Table 5.1. It was found that doping $TiCl_3$ significantly decreases the activation energy of both steps of the hydrogen desorption of $NaAlH_4$. In the 1st desorption, the Ea value of $NaAlH_4$ clearly decreases from 118 kJ $mol^{-1}H_2$ to 75 kJ $mol^{-1}H_2$ ($TiCl_3$-$NaAlH_4$). In the case of the 2nd decomposition, the Ea value also decreases from 120.7 kJ $mol^{-1}H_2$ for pristine $NaAlH_4$ to 101 kJ $mol^{-1}H_2$ for $TiCl_3$-$NaAlH_4$. This indicates that doping $TiCl_3$ would help the decomposition of Al-H bond in the $[AlH_4]^{-1}$ and $[AlH_6]^{-3}$ by lowering the activation energy in the hydrogen desorption. The frequency factors of both steps of the hydrogen desorption of $TiCl_3$-$NaAlH_4$ are lower than that of $NaAlH_4$.

5.5 Conclusion

The hydrogen desorption/re-absorption of $NaAlH_4$ doped with TiO_2 or metallic Ti was performed. It was found that TiO_2 doped $NaAlH_4$ exhibits the similar behavior as $TiCl_3$ doped $NaAlH_4$ with the reversible hydrogen capacity about 3.8 wt% (H/M). In addition, TiO_2 also improves the rate of hydrogen re-absorption in the desorbed sample compared with that using $TiCl_3$. This is due to the porosity of TiO_2 facilitating the hydrogen diffusion in the desorbed sample. However, some TiO_2 is reduced by $NaAlH_4$ and produces by-products, which are NaOH and Na_2O. This may be one reason why the reversible hydrogen capacity of $NaAlH_4$ doped with TiO_2 is not different with that of $TiCl_3$ doped $NaAlH_4$. In the case of Ti doped $NaAlH_4$, only the hydrogen re-absorption of $3NaH+Al+3/2H_2 \rightarrow Na_3AlH_6$ can take place with the reversible hydrogen capacity of 1 wt% (H/M). It reveals that metallic Ti became as TiH_x ($1 < x < 2$) in the sample after hydrogen desorption/re-absorption. This may indicate that the formation of TiH_x decreases the activity in hydrogen dissociation in the desorbed sample.

5.6 Acknowledgements

This work was supported by the National Science and Technology Development Agency (Reverse Brain Drain Project); the Petroleum and Petrochemical College (PPC), the Research Unit for Petrochemical and Environment Catalysts, the Ratchadapisek Somphot Endowment, and National Center of Excellence for Petroleum, Petrochemicals and Advanced Materials, Chulalongkorn University; and UOP LLC.

5.7 References

[1] Satyapal S, Petrovic J, Read C, Thomas G, Ordaz G. The U.S. department of energy's national hydrogen storage project: progress towards meeting hydrogen-powered vehicle requirements. Catal. Today 2007:120;246-256.

[2] Schüth F, Bogdanović B, Felderhoff M. Light metal hydrides and complex hydrides for hydrogen storage. Chem. Comm. 2004:2249-2258.

[3] Bogdanović B, Schwickardi M. Ti-doped alkali metal aluminium hydrides as potential novel reversible hydrogen storage materials. J. Alloys Compd. 1997;253-254:1-9.

[4] Zidan A, Takara S, Hee A, Jensen CM. Hydrogen cycling behavior of zirconium and titanium-zirconium-doped sodium aluminum hydride. J. Alloys Compd. 1999;285:119-122.

[5] Jensen M, Zidan R, Mariels N, Hee A, Hagen C. Advance titanium doping of sodium aluminum hydride: segue to a pratical hydrogen storage material? Int. J. Hydrogen Energy 1999;24:461-465.

[6] Bogdanović B, Brand RA, Marjanovic A, Schwickardi M, Tolle J. Metal-doped sodium aluminium hydrides as potential new hydrogen storage materials. J. Alloys Compd. 2000;302:36-58.

[7] Sandrock G, Gross K, Thomas G. Effect of Ti-catalyst content on the reversible hydrogen storage properties of the sodium alanates. J. Alloys Compd. 2002;399:299-308.

[8] Gross KJ, Majzoub EH, Spangler SW. The effects of titanium precursors on hydriding properties of alanates. J. Alloys Compd. 2003;356-357:423-428.

[9] Anton DL. Hydrogen desorption kinetics in transition metal modified $NaAlH_4$. J. Alloys Compd. 2003;356-357:400-404.

[10] Suttisawat Y, Jannatisin V, Rangsunvigit P, Kitiyanan B, Muangsin N, Kulprathipanja S. Catalytic effect of Zr and Hf on hydrogen desorption/absorption of $NaAlH_4$ and $LiAlH_4$. Int. J. Hydrogen Energy 2007;32:1277-1285.

[11] Suttisawat Y, Jannatisin V, Rangsunvigit P, Kitiyanan B, Muangsin N, Kulprathipanja S. Understanding the effect of TiO_2, VCl_3, and $HfCl_4$ on hydrogen desorption/absorption of $NaAlH_4$. J. Power Sources 2007;163:997-1002.

[12] Sandrock G, Gross K, Thomas G, Jensen C, Meeker D, Takara S. Engineering consideration in the use of catalyzed sodium alanates for hydrogen storage. J. Alloys Compd. 2002, 330-332, 696-701.

[13] Barkhordarian G, Klassen T, Bormann R. Catalytic mechanism of transition-metal compound on Mg hydrogen sorption reaction. J. Phys. Chem. B, 2006, 110, 11020-11024.

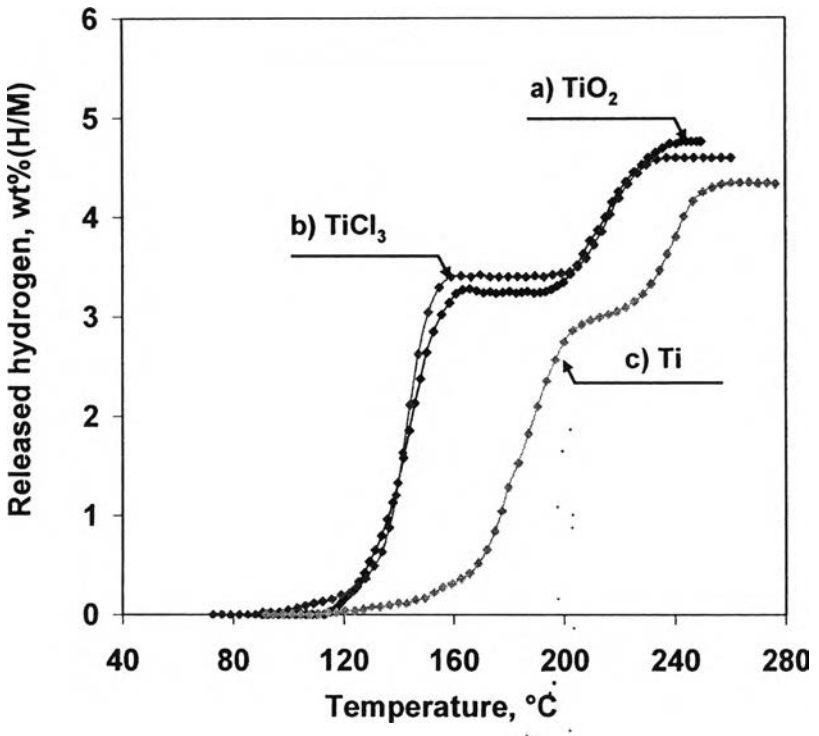

Figure 5.1 Correlation between temperature and hydrogen capacity, during the 1st hydrogen desorption on: a) TiO_2-$NaAlH_4$ b) $TiCl_3$-$NaAlH_4$, and c) Ti-$NaAlH_4$.

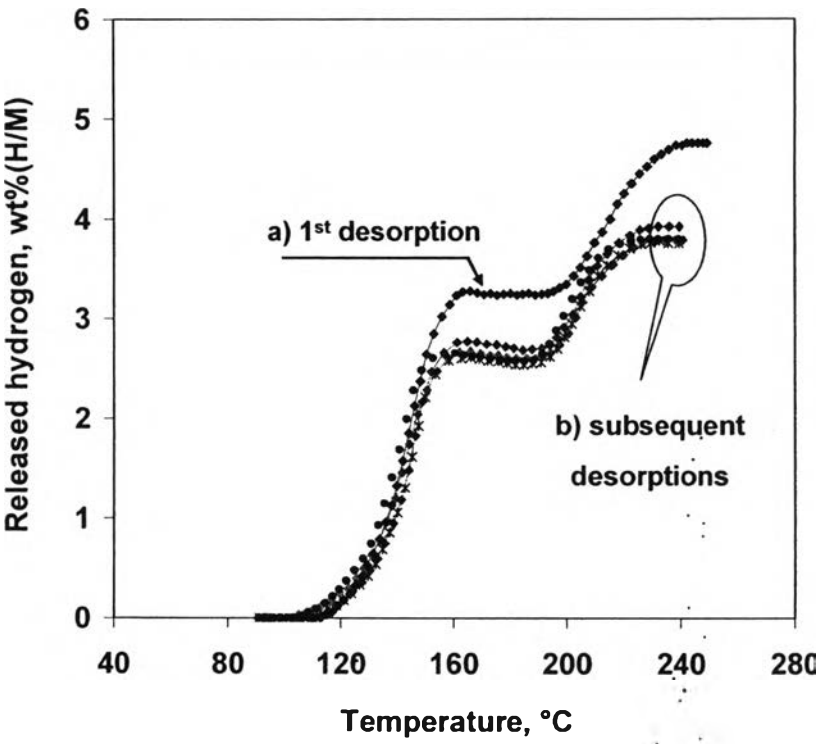

Figure 5.2 Correlation between temperature and hydrogen released during hydrogen desorption from $NaAlH_4$ doped with 4 mol% TiO_2 a) 1st desorption and b) subsequent desorptions.

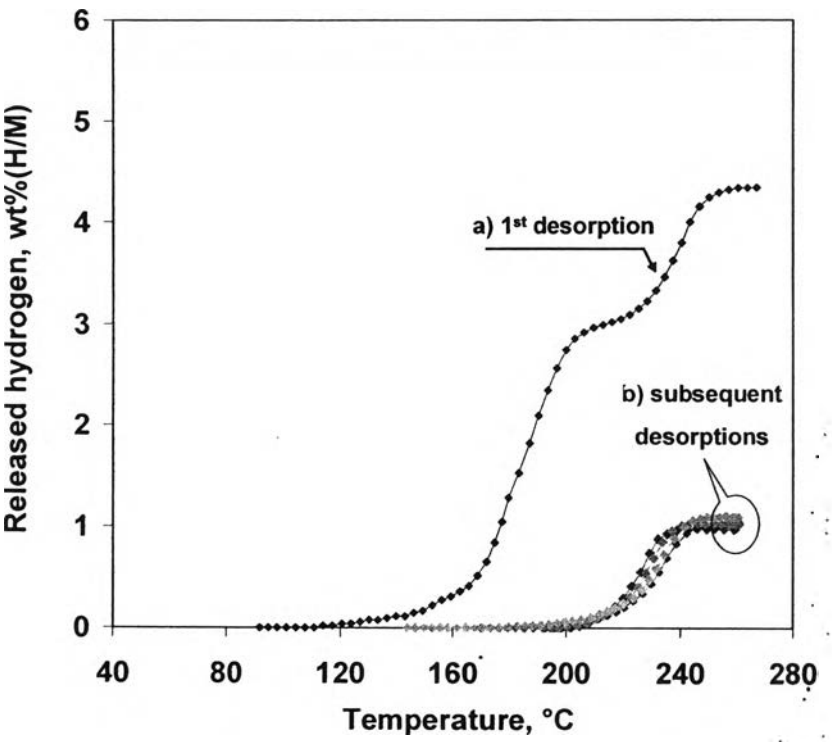

Figure 5.3 Correlation between temperature and hydrogen released during hydrogen desorption from $NaAlH_4$ doped with 4 mol% matallic Ti a) 1st desorption and b) subsequent desorptions.

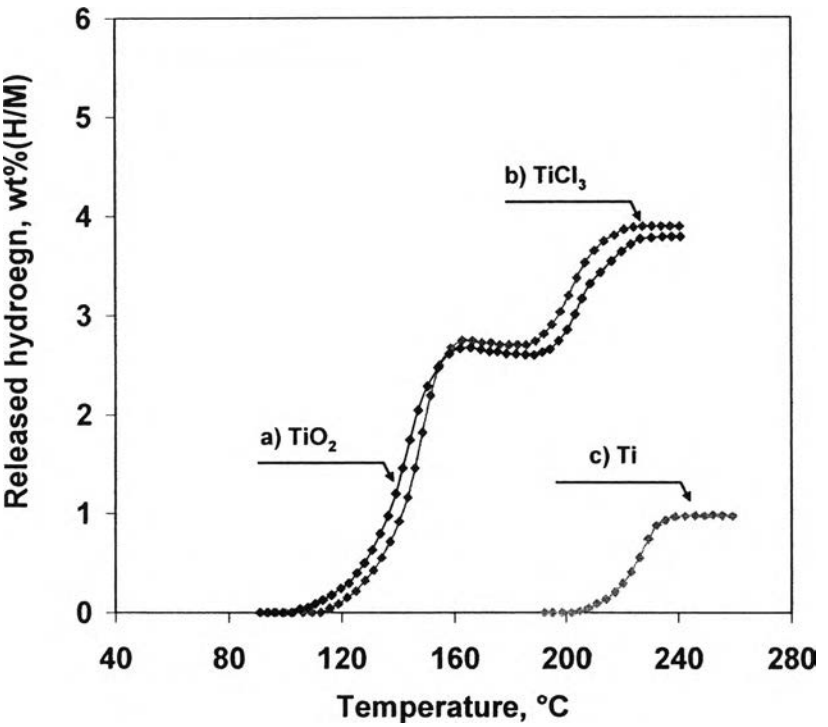

Figure 5.4 Comparison of the hydrogen desorption in the 7th desorption of a) TiO_2-$NaAlH_4$ b) $TiCl_3$-$NaAlH_4$, and c) Ti-$NaAlH_4$.

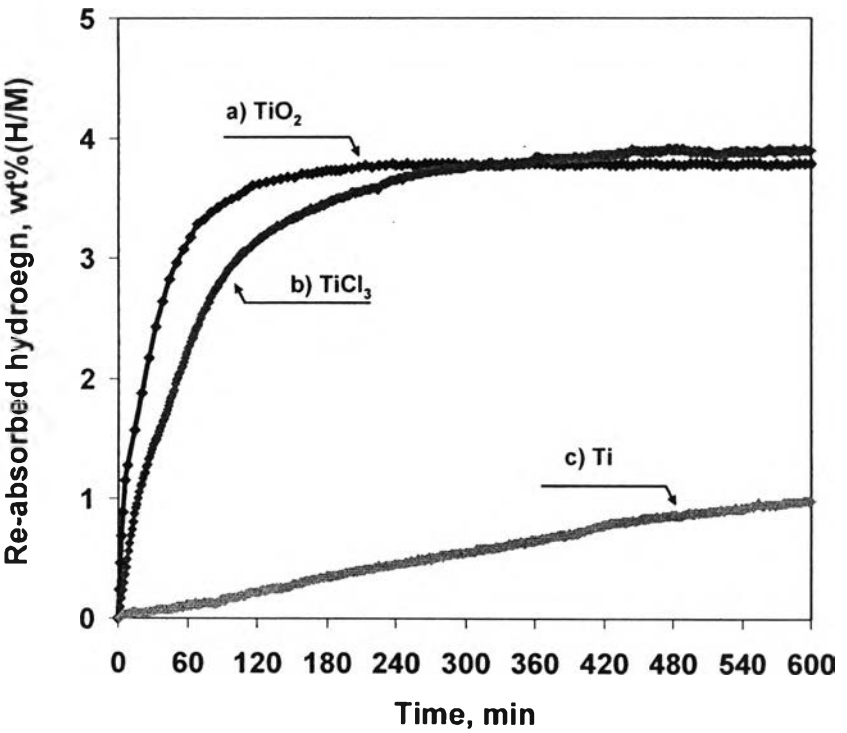

Figure 5.5 Hydrogen re-absorption rate of a) TiO_2-$NaAlH_4$, b) $TiCl_3$-$NaAlH_4$, and c) Ti-$NaAlH_4$.

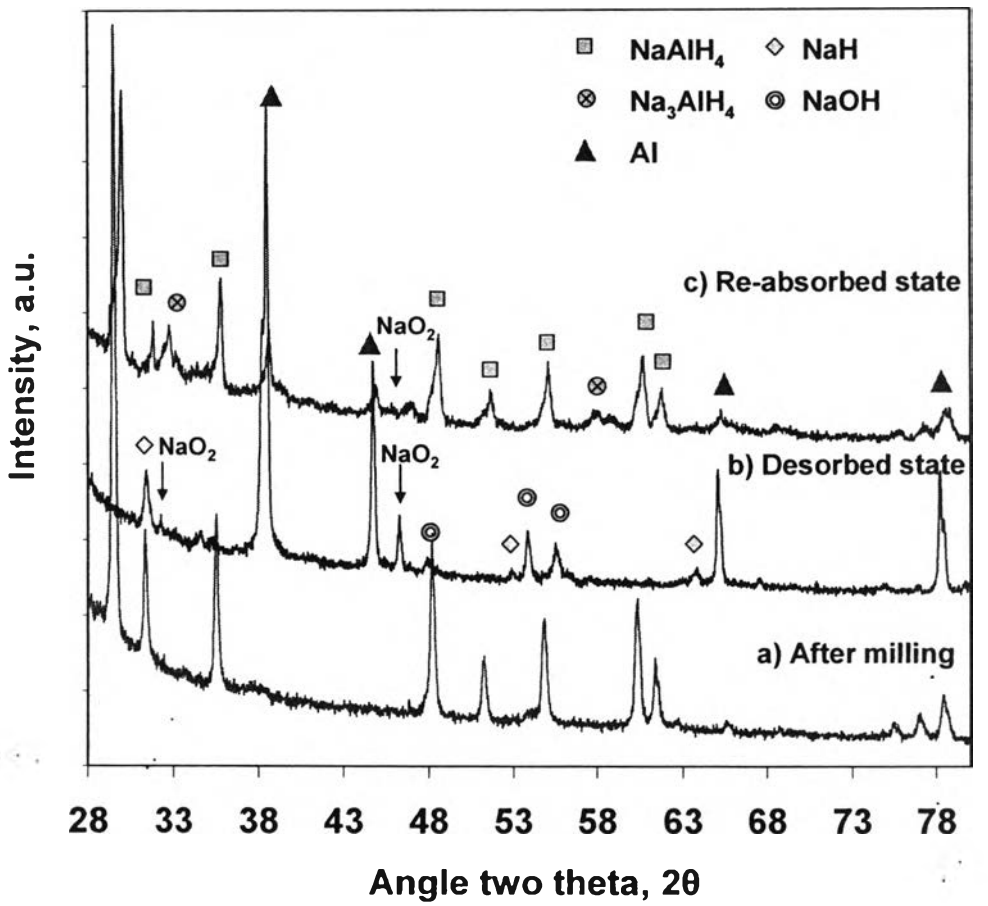

Figure 5.6 XRD patterns of 4 mol% TiO_2-$NaAlH_4$: a) after milling, b) after the hydrogen desorption, and after hydrogen re-absorption.

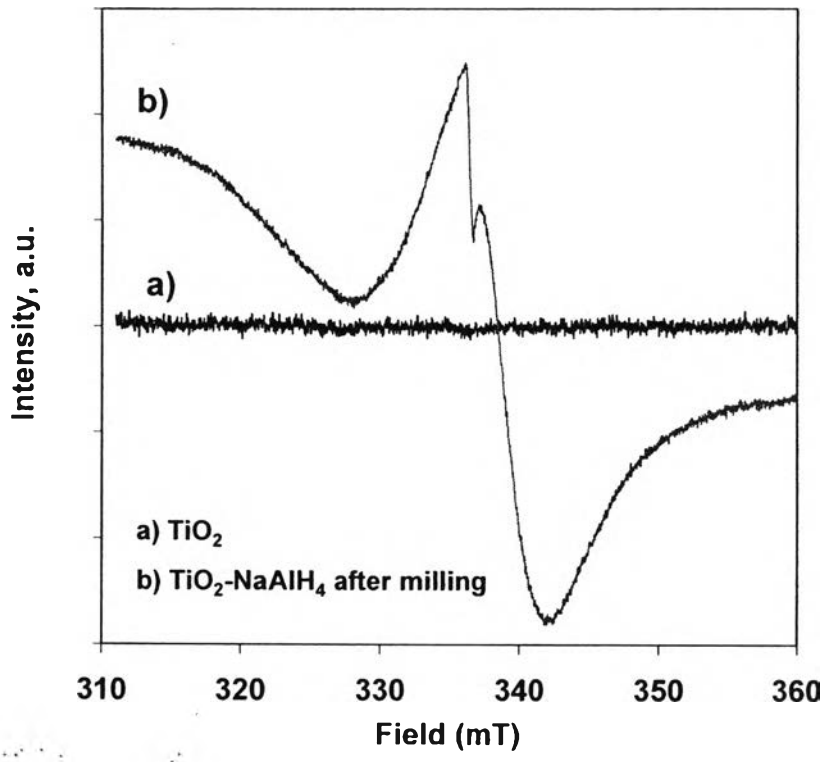

Figure 5.7 ESR patterns of a) as-received TiO_2 and b) TiO_2-$NaAlH_4$ after milling.

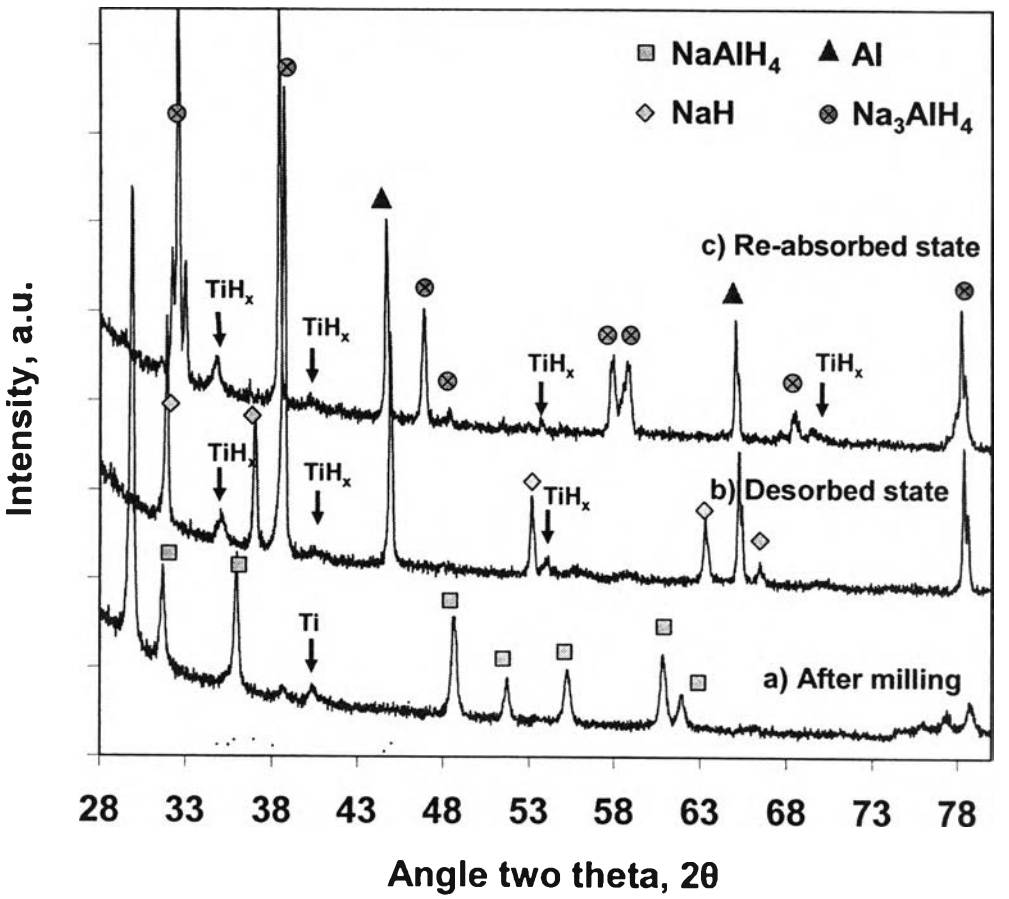

Figure 5.8 XRD patterns of 4 mol% Ti-$NaAlH_4$: a) after milling, b) after the hydrogen desorption, and after hydrogen re-absorption.

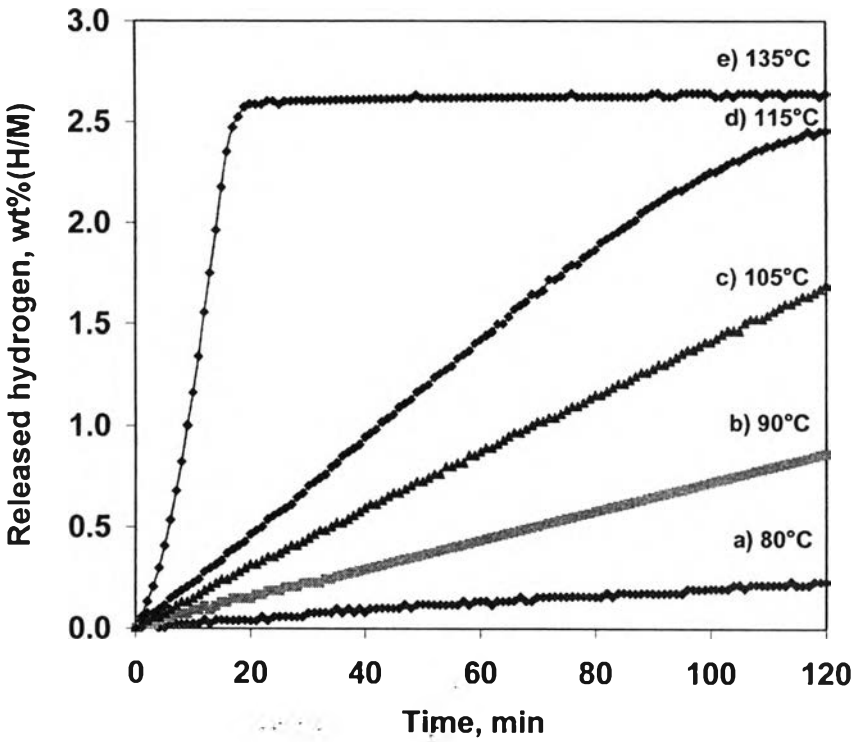

Figure 5.9 The isothermal hydrogen desorption of $TiCl_3$-$NaAlH_4$ in the 1st step decomposition at a) 80°C, b) 90°C, c) 105°C, d) 115°C, and e) 135°C.

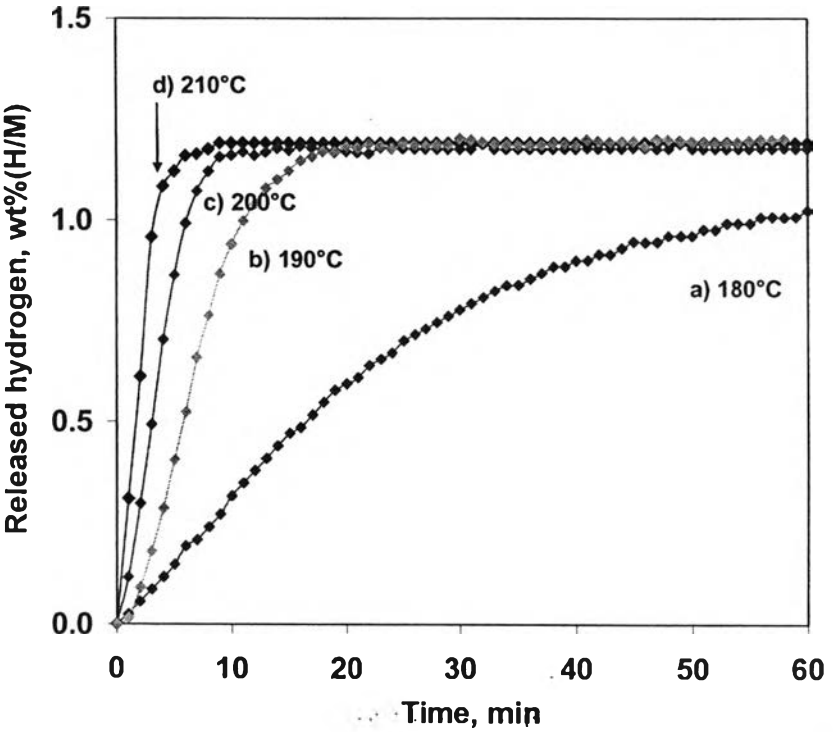

Figure 5.10 The isothermal hydrogen desorption of $TiCl_3$-$NaAlH_4$ in the 2nd step decomposition at a) 180°C, b) 190°C, c) 200°C, and d) 210°C.

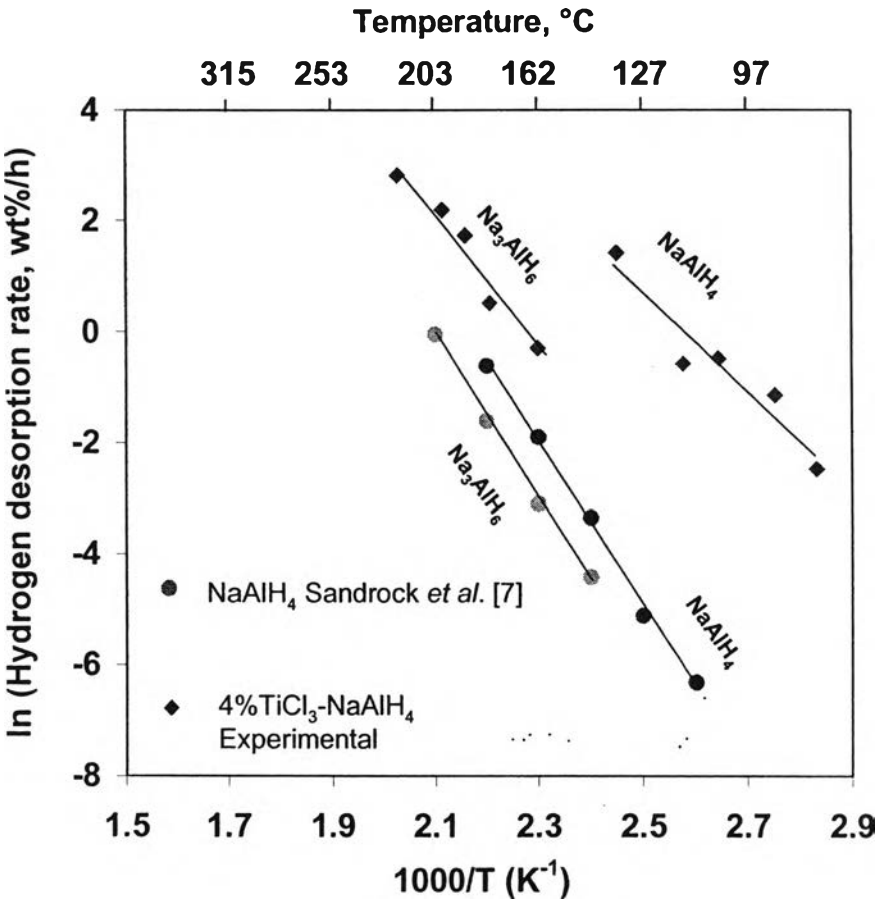

Figure 5.11 Arrhenius plot for $NaAlH_4$ and Na_3AlH_6 decomposition for $NaAlH_4$ [7] and 4 mol% $TiCl_3$ doped $NaAlH_4$.

Table 5.1 Experimentally derived parameter for the Arrhenius equation, k = A exp(-Ea/RT)

Sample	*Activation energy, Ea* $kJ\ mol^{-1}H_2$		*Frequency factor, A* $wt\%\ H_2\ h^{-1}$	
	$NaAlH_4$	Na_3AlH_6	$NaAlH_4$	Na_3AlH_6
undoped $NaAlH_4$ [7]	118.1	120.7	1.98×10^{13}	1.43×10^{13}
4%$TiCl_3$-$NaAlH_4$	74.63	101.01	1.12×10^{10}	1.02×10^{12}